Hyperspectral Image Classification and Dimensionality Reduction: An Orthogonal Subspace Projection Approach

Joseph C. Harsanyi, *Member, IEEE,* and Chein-I Chang, *Senior Member, IEEE*

Abstract—**Most applications of hyperspectral imagery require processing techniques which achieve two fundamental goals: 1) detect and classify the constituent materials for each pixel in the scene; 2) reduce the data volume/dimensionality, without loss of critical information, so that it can be processed efficiently and assimilated by a human analyst.**

In this paper, we describe a technique which simultaneously reduces the data dimensionality, suppresses undesired or interfering spectral signatures, and detects the presence of a spectral signature of interest. The basic concept is to project each pixel vector onto a subspace which is orthogonal to the undesired signatures. This operation is an optimal interference suppression process in the least squares sense. Once the interfering signatures have been nulled, projecting the residual onto the signature of interest maximizes the signal-to-noise ratio and results in a single component image that represents a classification for the signature of interest. The orthogonal subspace projection (OSP) operator can be extended to k signatures of interest, thus reducing the dimensionality of k and classifying the hyperspectral image simultaneously. The approach is applicable to both spectrally pure as well as mixed pixels.

I. Introduction

HYPERSPECTRAL imaging spectrometer data provide a wealth of information which can be used to address a variety of earth remote sensing problems. A short list of applications includes environmental mapping, global change research, geological research, wetlands mapping, assessment of trafficability, plant and mineral identification and abundance estimation, crop analysis, and bathymetry. The common theme in all of these applications is the requirement for classification of each pixel in the scene, and reduction of data volume to tractable levels.

Classification of a hyperspectral image sequence amounts to identifying which pixels contain various spectrally distinct materials that have been specified by the user. Several techniques for classification of multi/hyperspectral pixels have been used from minimum distance and maximum likelihood classifiers [1] to correlation/matched filter-based approaches such as spectral signature matching [2] and the spectral angle mapper [3]. The statistically based classifiers are limited since they do not account for the prevalent case of mixed pixels which are pixels that contain multiple spectral classes. Existing correlation/matched filter-based approaches suffer from the mixed pixel problem, as well as the limitation that the output of the matched filter is nonzero and quite often large for multiple classes since the spectral signatures of materials are not generally orthogonal vectors.

To reduce the data volume, techniques for reducing the image dimensionality are often applied. Typically, the dimensionality of a hyperspectral image cube is reduced by applying a linear transformation, such as a principal components transformation, and retaining only the significant components for further processing. The principal components transformation produces a new set of uncorrelated images that are ordered in terms of decreasing information or, equivalently, decreasing variance [4]. Although each hyperspectral pixel is a high (>100) dimensional vector, most of the information about the scene can be described by a few (generally less than ten) dimensions. This reduced dimensionality is known as the intrinsic dimensionality [5]. A recent improvement to the principal components transformation is the noise-adjusted principal components transformation [6]. This transformation orders the new images in terms of signal-to-noise ratio, and thus deemphasizes noise in the resulting images [7].

Although these approaches are sufficient for reducing data volume, they do not emphasize individual spectral classes or signatures of interest. For example, the first principal component image contains the most information/variance, but it is generally a linear combination of information from several spectral classes. This is a direct consequence of the fact that most materials resident in hyperspectral scenes have spectral signatures that are correlated, whereas the eigenvectors used to derive the principal component images are, of course, orthogonal.

In this paper, we describe a technique which simultaneously reduces data dimensionality to a user-prescribed level and produces a new sequence of images which highlight the presence of each signature of interest. These new component images represent class maps for each of the signatures of interest. The technique is based on the concept of orthogonal subspace projection which is a result from the theory of least squares and has been further developed in the sensor array processing community [8], [9].

Manuscript received March 2, 1993; revised August 13, 1993 and March 15, 1994.

J. Harsanyi is with Applied Signal & Image Technology Company, Pasadena, MD, 21122.

C-I. Chang is with the Department of Electrical Engineering, University of Maryland, Baltimore County, Baltimore, MD 21228.

IEEE Log Number 9402661.

An equivalent result directed at image sequence processing has also been developed using the concept of simultaneous diagonalization (SD) filtering [10]. The technique presented here recasts the results from [8]–[10] into an intuitive two-step development. First, we determine the matrix operator which eliminates undesired or interfering signatures and is an optimal interference rejection process in the least squares sense. Second, we develop a vector operator which maximizes the residual desired signature signal-to-noise ratio (SNR). A combination of these operators into an overall OSP classification operator reduces the non-Gaussian detection and classification problem presented by mixed pixels to the solved problem of detecting an unknown constant in white noise.

The rest of the paper is organized as follows. Section II covers formulation of the problem. Section III introduces the concept of orthogonal subspace projection, and introduces the hyperspectral pixel classification operator. Results of simulations and application of the operator to AVIRIS data are presented in Sections IV and V, respectively, and concluding remarks are given in Section VI.

II. Problem Formulation

A hyperspectral image cube is made up of hundreds of spatially registered images, taken contiguously over a large wavelength region, with high (<10 nm) spectral resolution [11]. Each pixel in a hyperspectral image cube is an observation vector which represents the reflected energy spectrum of the materials within the spatial area covered by the pixel. Existing hyperspectral sensors produce observation vectors that have several hundred elements. For example, each pixel from the NASA/JPL Airborne Visible/Infrared Imaging Spectrometer (AVIRIS) contains 224 elements corresponding to 224 spectral wavelength bands ranging from 0.4 to 2.5 μm. Each spectral band has approximately a 10 nm bandwidth.

Generally, the spatial coverage of each pixel may encompass several different materials, each with a unique spectral signature. In this case, the observation vector is affected by the individual spectral signatures of each material, and the pixel is termed mixed [4], [5]. A mixed pixel containing p spectrally distinct materials, denoted by the $l \times 1$ vector $\boldsymbol{r}(x, y)$, can be described by the linear model

$$\boldsymbol{r}(x, y) = \boldsymbol{M}\boldsymbol{\alpha}(x, y) + \boldsymbol{n}(x, y) \tag{1}$$

where l is the number of spectral bands, (x, y) is the spatial position of the pixel, $\boldsymbol{M} = (\boldsymbol{u}_1 \cdots \boldsymbol{u}_i \cdots \boldsymbol{u}_{p-1}, \boldsymbol{d})$ is an $l \times p$ matrix with linearly independent columns and the $l \times 1$ column vector $\boldsymbol{u}_i$ is the spectral signature of the ith distinct material, $\boldsymbol{\alpha}(x, y)$ is a $p \times 1$ vector where the ith element represents the fraction of the ith signature present in the pixel, and $\boldsymbol{n}(x, y)$ is an $l \times 1$ vector representing random noise which is assumed to be an independent, identically distributed (i.i.d.) Gaussian process with zero mean and covariance matrix $\sigma^2 I$.

Without loss of generality, we assume that the last column of $\boldsymbol{M}$ is the desired signature of interest which is denoted by $\boldsymbol{d}$. The remaining columns are undesired signatures denoted by $\boldsymbol{U} = (\boldsymbol{u}_1 \cdots \boldsymbol{u}_i \cdots \boldsymbol{u}_{p-1})$ that are assumed to be linearly independent. An equivalent statement of (1) which separates the desired and undesired signatures is given by

$$\boldsymbol{r} = \boldsymbol{d}\alpha_p + \boldsymbol{U}\boldsymbol{\gamma} + \boldsymbol{n}. \tag{2}$$

Here, we have suppressed the spatial position of the pixel for convenience, α_p is the fraction of the desired signature, and $\boldsymbol{\gamma}$ is a vector which contains the first $p-1$ elements of $\boldsymbol{\alpha}$.

We now develop an operator which eliminates the effects of $\boldsymbol{U}$ and maximizes the remaining signal energy with respect to the noise.

III. Hyperspectral Pixel Classification

A. Interference Rejection by Orthogonal Subspace Projection

The first step in deriving a classification operator for the signature of interest $\boldsymbol{d}$ is to eliminate the effects of interfering signatures which are represented by the columns of $\boldsymbol{U}$. The approach is to form an operator that projects $\boldsymbol{r}$ onto a subspace that is orthogonal to the columns of $\boldsymbol{U}$. The vector resulting from such an operation will only contain energy associated with the desired signature $\boldsymbol{d}$ and random noise. The least squares optimal interference rejection operator is given by the $l \times l$ matrix

$$\boldsymbol{P} = (\boldsymbol{I} - \boldsymbol{U}\boldsymbol{U}^{\#}) \tag{3}$$

where $\boldsymbol{U}^{\#} = (\boldsymbol{U}^T\boldsymbol{U})^{-1}\boldsymbol{U}^T$ is the pseudoinverse of $\boldsymbol{U}$. This operator has the same structure as the orthogonal complement projector from the theory of least squares [9] and the signal blocking matrix which has been used in the sensor array processing community [8]. In the case at hand, however, the operator minimizes energy associated with the signatures not of interest as opposed to minimizing the total least squares error. Operating on (2), we have

$$\boldsymbol{P}\boldsymbol{r} = \boldsymbol{P}\boldsymbol{d}\alpha_p + \boldsymbol{P}\boldsymbol{n}. \tag{4}$$

It is clear that this approach is an optimal interference rejection process in the least squares sense since $\boldsymbol{P}$ reduces the contribution of $\boldsymbol{U}$ to zero. Additional information regarding orthogonal subspace projection operators and their properties can be found in [8]–[10], [12], and [13].

B. Signal-to-Noise Ratio (SNR) Maximization

The second step in deriving the pixel classification operator is to find the $1 \times l$ operator $\boldsymbol{x}^T$ which maximizes the SNR. Operating on (4), we have

$$\boldsymbol{x}^T\boldsymbol{P}\boldsymbol{r} = \boldsymbol{x}^T\boldsymbol{P}\boldsymbol{d}\alpha_p + \boldsymbol{x}^T\boldsymbol{P}\boldsymbol{n} \tag{5}$$

which is a scalar. The signal-to-noise-energy ratio is given by

$$\lambda = \frac{\boldsymbol{x}^T\boldsymbol{P}\boldsymbol{d}\alpha_p^2\boldsymbol{d}^T\boldsymbol{P}^T\boldsymbol{x}}{\boldsymbol{x}^T\boldsymbol{P}E\{\boldsymbol{n}\boldsymbol{n}^T\}\boldsymbol{P}^T\boldsymbol{x}} = \frac{\alpha_p^2}{\sigma^2}\frac{\boldsymbol{x}^T\boldsymbol{P}\boldsymbol{d}\boldsymbol{d}^T\boldsymbol{P}^T\boldsymbol{x}}{\boldsymbol{x}^T\boldsymbol{P}\boldsymbol{P}^T\boldsymbol{x}} \tag{6}$$

where $E\{\cdot\}$ denotes the expected value.

Maximization of this quotient is the generalized eigenvector problem

$$\boldsymbol{P}\boldsymbol{d}\boldsymbol{d}^T\boldsymbol{P}^T\boldsymbol{x} = \tilde{\lambda}\boldsymbol{P}\boldsymbol{P}^T\boldsymbol{x} \tag{7}$$

where $\tilde{\lambda} = \lambda(\sigma^2/\alpha_p)$. The value of $\boldsymbol{x}^T$ which maximizes $\tilde{\lambda}$ can be determined in general using techniques outlined in [10] and the idempotent ($\boldsymbol{P}^2 = \boldsymbol{P}$) and symmetric ($\boldsymbol{P}^T = \boldsymbol{P}$) properties of the interference rejection operator. The result is

$$\boldsymbol{x}^T = \kappa\boldsymbol{d}^T \tag{8}$$

where κ is an arbitrary scalar.

C. Orthogonal Subspace Projection (OSP) Classification Operator

Substituting the result in (8) into (5), we see that the overall classification operator for a desired hyperspectral signature in the presence of multiple undesired signatures and white noise is given by the $1 \times l$ vector

$$\boldsymbol{q}^T = \boldsymbol{d}^T\boldsymbol{P}. \tag{9}$$

This is an intuitively pleasing result since it first nulls the interfering signatures, and then uses a matched filter for the desired signature to maximize the SNR. The operator is similar to a result from the sensor array processing community which is used for higher rank spectrum estimation or, equivalently, estimation of the SNR for a candidate multiemitter matched filter [9]. It is also one of the limiting special cases that is derived in [10] for the simultaneous diagonalization (SD) filter with noise variance equal to zero. Finally, the operator can be shown to provide least squares optimal fraction images [12] that are equivalent to those produced by linear mixture modeling techniques [4], [5], [14]–[18].

An interesting consequence of the two-step development approach that we have used to arrive at this result is to show that the equivalent SD filter for the zero noise variance case is also the least squares optimal interference rejection/max SNR filter for the case when white noise is present with variance σ^2. This is important from an automatic detection perspective since this operator reduces the non-Gaussian mixed pixel classification problem to the problem of detecting the unknown constant $\boldsymbol{d}^T\boldsymbol{P}\boldsymbol{d}\alpha_p$ in the presence of white noise.

When the operator in (9) is applied to all of the pixels in a hyperspectral scene, each $l \times 1$ pixel is reduced to a scalar which is a measure of the presence of the signature of interest. The ultimate result is to reduce the l images comprising the hyperspectral image cube into a single image where pixels with high intensity indicate the presence of the desired signature. This represents a significant reduction in data volume since l is >200 for current and planned airborne hyperspectral sensors. Since the classification operator reduces each pixel to an unknown constant in white noise, the resultant image can be sensibly thresholded and an automatic binary classification decision can be made based on the Neyman–Pearson detection criterion [12], [19]. This criterion maximizes the probability of detecting the presence of the signature of interest subject to a user designated false alarm rate.

The extension of this vector operator for a single signature to a matrix operator for k signatures of interest is straightforward. The $k \times l$ matrix operator is given by

$$\boldsymbol{Q} = (\boldsymbol{q}_1 \cdots \boldsymbol{q}_i \cdots \boldsymbol{q}_k)^T \tag{10}$$

where each of the $\boldsymbol{q}_i^T = \boldsymbol{d}_i^T\boldsymbol{P}_i$ is formed with the appropriate desired and undesired signature vectors. In this case, the hyperspectral image cube is reduced to k images which classify each of the signatures of interest.

IV. Simulation Results

In this section, we present an application of the orthogonal subspace projection (OSP) technique to linearly mixed reflectance spectra. In the first case, 100 hyperspectral pixels were simulated using the red soil and dry grass reflectance spectra shown in Fig. 1. These spectra were first convolved to 10 nm spectral bands to simulate the capability of current airborne hyperspectral sensors. The abundance of each material varied from pixel to pixel, and white Gaussian noise was added to each pixel to achieve a 25 : 1 signal-to-noise ratio. The signal-to-noise ratio is defined here as 50% reflectance divided by the standard deviation of the noise. This should not be confused with the signal-to-noise-energy ratio which is maximized in (6) to develop the optimal classification operator. Pixels 20, 40, 60, and 80 also contain the creosote leaves reflectance spectrum, shown in Fig. 1, at 20, 15, 10, and 5% abundance, respectively. To illustrate the severity of the detection/classification problem, pixels 18–22 are shown in Fig. 2. Pixel 20, which contains the creosote leaves spectrum at 20% abundance, is not distinguishable from the neighboring pixels. The missing portions of the spectra are where the 1.4 and 1.9 μm water bands have been removed.

An OSP classification operator was formed using (9) where $\boldsymbol{d}$ is the creosote leaves spectrum and the two columns of $\boldsymbol{U}$ are the red soil and dry grass spectra. The result of applying the operator to each pixel is shown in Fig. 3. The pixels containing the creosote leaves spectrum are evident.

A second simulation was run using the reflectance spectra in Fig. 4. Again, 100 mixed pixels were simulated, and in this case, we form an operator to detect sage brush in the presence of both creosote leaves and black brush. As before, pixels 20, 40, 60, and 80 contain the target reflectance spectrum, sage brush, at 20, 15, 10, and 5% abundance, respectively. In this case, white Gaussian noise was added to each pixel to achieve a 50 : 1 signal-to-noise ratio referenced to 50% reflectance. The result of applying the operator to each pixel is shown in Fig. 5. This is clearly a more difficult classification problem than the first simulation, but the presence of the sage brush spectrum is detectable in all but the 5% abundance case.

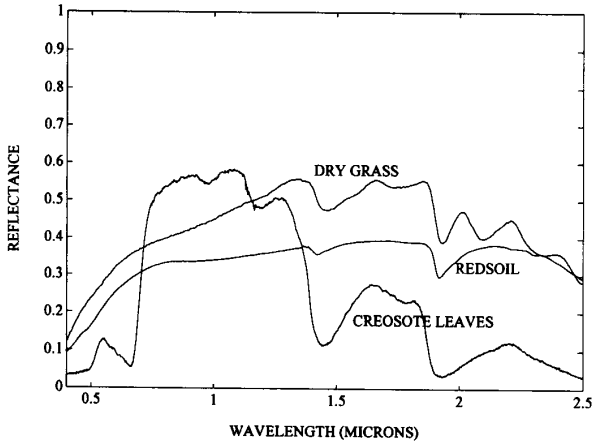

Fig. 1. Reflectance spectra: simulation 1.

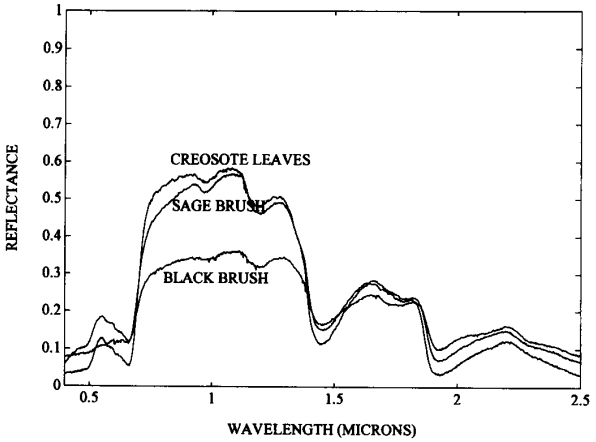

Fig. 4. Reflectance spectra: simulation 2.

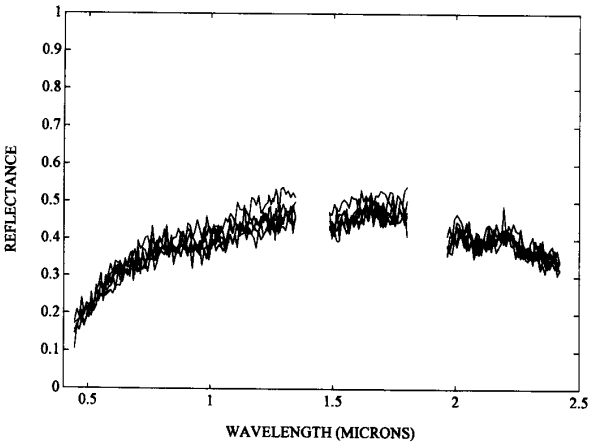

Fig. 2. Mixed spectra. This figure shows simulated pixels 18–22. Pixel 20, which contains the creosote leaves spectrum, is not distinguishable. Discontinuities in the spectra are where atmospheric water bands have been removed.

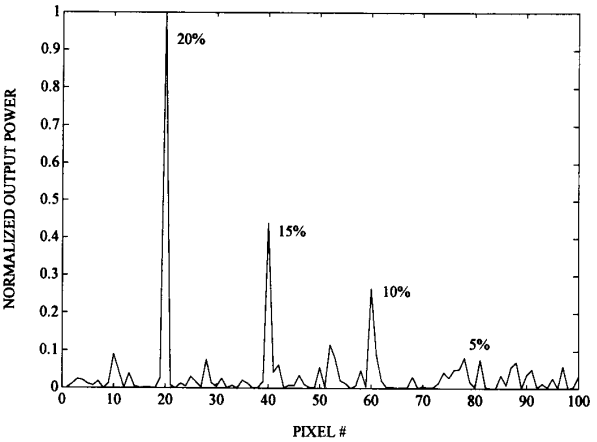

Fig. 5. OSP operator output: simulation 2. This result demonstrates the difficult problem of discrmination between spectrally similar vegetation. In this case, the sage brush spectrum is detectable in all but the 5% abundance case.

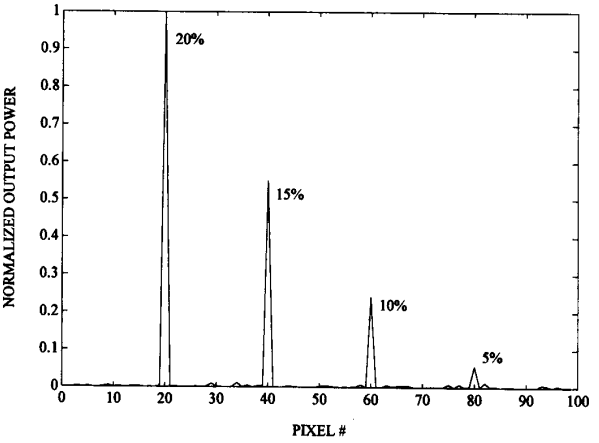

Fig. 3. OSP operator output: simulation 1. The result of operating on each pixel vector is a scalar. The relative output power for each pixel is shown as a function of pixel number. The presence of the creosote leaves spectrum is detectable to approximately 5% abundance in this case.

V. Experimental Results Using AVIRIS Data

The OSP technique was also applied to a subsection of an AVIRIS scene of the Lunar Crater Volcanic Field (LCVF) which is located in Northern Nye County, NV. Extensive field work has been done in this area, and the AVIRIS scene covering it has been previously modeled using spectral mixture analysis [20], [21]. A single band image from the AVIRIS data is shown in Fig. 6. Atmospheric water bands and low SNR bands have been removed from the data, reducing the image cube from 224 to 158 bands.

The signatures used to develop the OSP classification operator are the same image endmembers that were used to model the scene with spectral unmixing techniques in [20]. These endmembers, which are extracted directly from the image, are the radiance spectra of red oxidized basaltic cinders, rhyolite, playa, vegetation, and shade

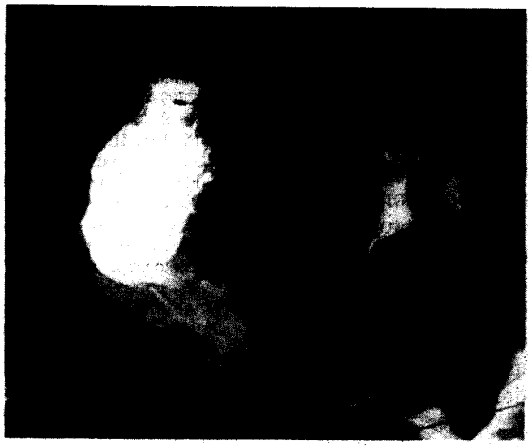

Fig. 6. AVIRIS image of the Lunar Crater Volcanic Field (0.752 μm channel).

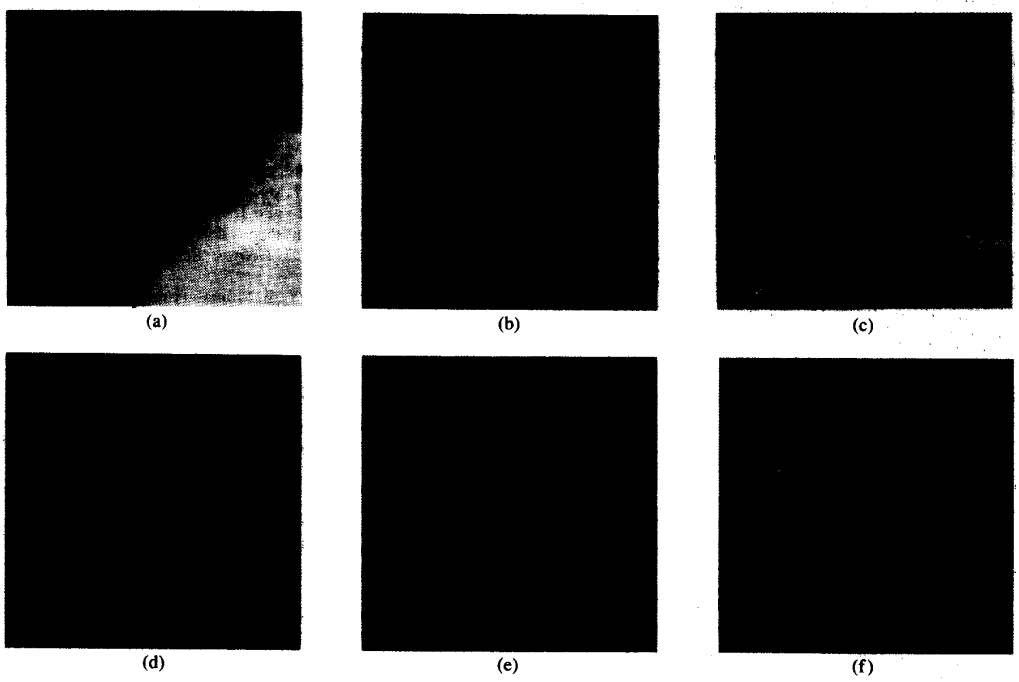

Fig. 7. OSP operator output: LCVF subsection. Operating on a 200 × 200 pixel subsection from the upper left corner of the LCVF, scene (a) yields component images for each of the chosen material image endmembers. The component image in (b) indicates the presence of red oxidized basaltic cinders, (c) clearly shows the dry playa lakebed, (d) indicates exposures of rhyolite, (e) shows vegetation, and (f) represents shade which accounts for variable lighting and topography. The data reduction provided by the operator in this case is from a 158 band hyperspectral image cube to five component images which provide information of interest regarding the chosen image endmembers.

which accounts for topographic shadowing and variable lighting geometries within the scene. It is important to note that it is not necessary to calibrate the AVIRIS data to reflectance before applying the orthogonal subspace approach. In this case, we develop an operator based on radiance spectra, and operate directly on the measured radiance for each pixel in the scene.

For this experiment, we develop the classification operator for each of the image endmembers as in (10). Applying the overall operator to the image results in a dimensionality reduction in this case of 158 to 5. The resultant component images for each of the endmembers are shown in Fig. 7. These component images represent class maps of the various endmembers, and are consistent with known attributes of the scene which have been determined by field observations and mapping [20], [22].

VI. Conclusion

An approach for simultaneously reducing hyperspectral data dimensionality and detecting hyperspectral signatures of interest in the presence of undesired or interfering signatures has been developed and demonstrated. The technique can be viewed as a combination of two linear operators into a single classification operator. The first operator is an optimal interference rejection process in the least squares sense, and the second is an optimal detector in the maximum SNR sense. The approach is applicable to both mixed pixels as well as spectrally pure pixels, and does not suffer from the limitations of standard statistical classifiers and matched filtering/spectral signature matching techniques which are suboptimal in the presence of multiple correlated interferers.

Application of the technique to simulated hyperspectral mixed pixels shows that representative signatures of interest can be detected at abundance levels as low as a few percent at signal-to-noise ratios ($\leq 50:1$) and spectral resolution (10 nm) which are easily attainable with existing airborne hyperspectral sensors. Performance will, of course, vary depending on the particular scenario, but this technique can be used as an analysis tool to examine the sensor capabilities required to solve a particular detection and classification problem.

The technique has also been applied to data collected with the Airborne Visible/Infrared Imaging Spectrometer (AVIRIS) from the Lunar Crater Volcanic Field (LCVF) in Nevada. The technique produces component images which represent class maps of the various materials of interest within the scene. Component images generated for the LCVF scene are reasonable when compared to published geologic maps of the area [23] and corroborating field observations [20].

Acknowledgment

Laboratory sample spectra were obtained from Brown University's RELAB and the University of Washington (vegetation spectra). AVIRIS data of the Lunar Crater Volcanic Field were provided by the Planetary Data System of the National Space Science Data Center, Principal Investigator: R. Arvidson. Special thanks to W. Farrand of Science Applications International Corporation for providing geological interpretation of the results in Section V. The authors are also grateful to J. Hejl of the Applied Signal and Image Technology Company for many useful comments on drafts of this manuscript.

References

[1] P. Swain and S. Davis, Ed., *Remote Sensing: The Quantitative Approach*. New York: McGraw-Hill, 1983.

[2] A. S. Mazer, M. Martin *et al.*, "Image processing software for imaging spectrometry data analysis," *Remote Sensing Environ.*, vol. 24, no. 1, pp. 201–210, 1988.

[3] R. H. Yuhas, A. F. H. Goetz, and J. W. Boardman, "Discrimination among semi-arid landscape endmembers using the spectral angle mapper (SAM) algorithm," *Summaries 3rd Annu. JPL Airborne Geosci. Workshop*, June 1992, R. O. Green, Ed., Publ. 92-14, vol. 1, Jet Propulsion Laboratory, Pasadena, CA, 1992, pp. 147–149.

[4] M. O. Smith, P. E. Johnson, and J. B. Adams, "Quantitative determination of mineral types and abundances from reflectance spectra using principal components analysis," in *Proc. 15th Lunar and Planetary Sci. Conf., Part 2, Geophys. Res.*, vol. 90, suppl., pp. C797–C804, Feb. 15, 1985.

[5] A. R. Gillespie, M. O. Smith, J. B. Adams, S. C. Willis, A. F. Fischer, III, and D. E. Sabol, "Interpretation of residual images: Spectral mixture analysis of AVIRIS images, Owens Valley, California," in *Proc. 2nd AVIRIS Workshop*, R. O. Green, Ed., JPL Publ. 90-54, 243-270.

[6] J. B. Lee, A. S. Woodyatt, and M. Berman, "Enhancement of high spectral resolution remote sensing data by a noise-adjusted principal components transform," *IEEE Trans. Geosci. Remote Sensing*, vol. 28, pp. 295–304, May 1990.

[7] A. A. Green, M. Berman, P. Switzer, and M. Craig, "A transformation for ordering multispectral data in terms of image quality with implications for noise removal," *IEEE Trans. Geosci. Remote Sensing*, vol. 26, pp. 65–74, Jan. 1988.

[8] S. Haykin, Ed., *Advances in Spectrum Analysis and Array Processing, Volume II*. Englewood Cliffs, NJ: Prentice-Hall, 1991.

[9] —, *Adaptive Filter Theory*, 2nd ed. Englewood Cliffs, NJ: Prentice-Hall, 1991.

[10] J. W. V. Miller, J. B. Farison, and Y. Shin, "Spatially invariant image sequences," *IEEE Trans. Image Processing*, vol. 1, pp. 148–161, Apr. 1992.

[11] G. Vane and A. F. H. Goetz, "Terrestrial imaging spectroscopy," *Remote Sensing Environ.*, vol. 24, no. 1, pp. 1–29, 1988.

[12] J. C. Harsanyi, "Detection and classification of subpixel spectral signatures in hyperspectral image sequences," Ph.D. dissertation, Univ. Maryland, Baltimore County, 116 pp., 1993.

[13] G. H. Golub and C. F. Van Loan, *Matrix Computations*. Baltimore: Johns Hopkins Univ. Press, 1983.

[14] J. B. Adams and M. O. Smith, "Spectral mixture modeling: A new analysis of rock and soil types at the Viking Lander 1 site," *J. Geophys. Res.*, vol. 91, pp. 8098–8112, July 1986.

[15] Y. E. Shimabukuro and J. A. Smith, "Least squares mixing models to generate fraction images derived from remote sensing multispectral data," *IEEE Trans. Geosci. Remote Sensing*, vol. 29, pp. 16–20, Jan. 1991.

[16] B. N. Holben and Y. E. Shimabukuro, "Linear mixing model applied to coarse spatial resolution data from multispectral satellite sensors," *Int. J. Remote Sensing*, vol. 14, no. 11, pp. 2231–2240, 1993.

[17] D. E. Sabol, J. B. Adams, and M. O. Smith, "Quantitative subpixel spectral detection of targets in multispectral images," *J. Geophys. Res.*, vol. 97, pp. 2659–2672, Feb. 25, 1992.

[18] A. R. Huete, "Separation of soil-plant spectral mixtures by factor analysis," *Remote Sensing Environ.*, vol. 19, no. 1, pp. 237–251, 1986.

[19] H. V. Poor, *An Introduction to Signal Detection and Estimation*, New York: Springer-Verlag, 1988.

[20] W. H. Farrand, "Visible and near infrared reflectance of tuff rings and tuff cones," Ph.D. dissertation, Univ. Arizona, Tucson, 1991.

[21] W. H. Farrand and R. B. Singer, "Analysis of altered volcanic pyroclasts using AVIRIS data," in *Proc. 3rd Airborne Visible/Infrared Imaging Spectrometer (AVIRIS) Workshop*, JPL Publ. 91-28, Jet Propulsion Lab., Pasadena, CA, 1991.

[22] D. H. Scott and N. J. Trask, "Geology of the Lunar Crater Volcanic Field, Nye County, Nevada," USGS Prof. Paper 599-I, 1971.

[23] R. P. Snyder, E. B. Ekren, and G. L. Dixon, "Geologic map of the Lunar Crater Quadrangle, Nye County, Nevada," USGS Misc. Geol. Inv. Map I-700, scale 1:48000, 1972.

Joseph C. Harsanyi was born is Syracuse, NY on November 17, 1962. He received the B.A. degree from the University of Maryland, Baltimore County in 1985, the M.S.E.E. from Johns Hopkins University in 1988, and the Ph.D. degree from the University of Maryland, Baltimore County in 1993.

Since 1985, Dr. Harsanyi has been working in private industry in the areas of digital and optical signal processing with applications to signal detection, characterization, and direction finding.

In 1992 Dr. Harsanyi co-founded Applied Signal and Image Technology Co. which specializes in the application of signal processing theory to problems in the areas of airborne direction finding and earth remote sensing. His current research interests include adaptive array signal processing theory and application, hyperspectral image sequence processing and medical signal and image processing.

Chein-I Chang (S'81-M'87-SM'92) received the B.S., M.S., and M.A. degrees from Soochow University, Taipei, Taiwan, in 1973, National Tsing Hua University, Hsinchu, Taiwan in 1975, and SUNY at Stony Brook in 1977, respectively, all in mathematics, and the M.S.E.E. degree from the University of Illinois at Urbana-Champaign in 1982, and the Ph.D. degree in electrical engineering from the University of Maryland, College Park, in 1987.

From 1973 to 1977 he was a Teaching Assistant at Soochow University, National Tsing Hua University and SUNY at Stony Brook. From 1977 to 1980 he was an Instructor of Mathematics at the University of Illinois. During 1980-1982 he was a Research Assistant at the University of Illinois, and was also a Research Assistant at the University of Maryland from 1982 to 1986. He was a Visiting Assistant Professor from January 1987 to August 1987, Assistant Professor from 1987 to 1993, and is currently Associate Professor in the Department of Electrical Engineering at the University of Maryland, Baltimore County. His research interests include information theory and coding, signal detection and estimation, biomedical signal/imaging processing, multispectral/hyperspectral signal and image processing, sensor/data fusion, neural networks, computer vision, and pattern recognition.

Dr. Chang is a member of the SPIE, the International Neural Network Society, Phi Kappa Phi, and Eta Kappa Nu.